First statistics of the isopistonic angle for long baseline interferometry

A. Ziad, T. Elhalkouj, R. Petrov, J. Borgnino, M. Lazrek, Z. Benkhaldoun, F. Martin, Y. Elazhari

Monthly Notices
of the
ROYAL ASTRONOMICAL SOCIETY

MNRAS **458,** 4044–4051 (2016)
Advance Access publication 2016 March 7

doi:10.1093/mnras/stw366

First statistics of the isopistonic angle for long baseline interferometry

A. Ziad,[1⋆] T. Elhalkouj,[2⋆] R. G. Petrov,[1⋆] J. Borgnino,[1] M. Lazrek,[2] Z. Benkhaldoun,[2] F. Martin[1] and Y. Elazhari[2]

[1]*Laboratoire J.L. Lagrange, Université Côte d'Azur/OCA/CNRS, Parc Valrose, F-06108 Nice, France*
[2]*Laboratoire LPHEA, Oukaimeden Observatory, Cadi Ayyad University/FSSM, BP 2390, Marrakesh, Morocco*

Accepted 2016 February 12. Received 2016 February 11; in original form 2015 October 2

ABSTRACT

To reach a suitable limiting magnitude with a multi-aperture interferometer, we need to cophase the different telescopes using a reference source. The latter should be located in the same isopistonic domain as the science source. We developed a direct analytical expression of deducing the isopistonic angle from atmospheric optical parameters as seeing, isoplanatic angle and outer scale. All of these atmospheric turbulence parameters are measured by the Generalized Seeing Monitor (GSM). The first statistics of the isopistonic angle obtained from the GSM data are presented and comparison between the major sites over the world are discussed (La Silla, Cerro Pachon, Paranal, San Pedro, Mt Palomar, Mauna Kea, La Palma, Oukaïmeden, Maydanak, Dome C). Implications of these isopistonic angle statistics on large interferometers cophasing in terms of sky coverage and limiting magnitude are discussed.

Key words: atmospheric effects – instrumentation: high angular resolution – instrumentation: interferometers – site testing.

1 INTRODUCTION

The atmospheric turbulence parameters have a strong impact on high angular resolution techniques such as adaptive optics and interferometry. Indeed, design, performance and optimization of large baseline interferometers (LBI) and adaptive optics systems are related to atmospheric considerations and notably to the seeing, the wavefront outer scale amplitude and the isoplanatic domain. Several analyses of seeing and outer scale effects in terms of Zernike decomposition of the atmospherically induced phase aberrations were performed theoretically (Winker 1991). In interferometry, the fringe excursion is strongly dependent on the outer scale according to the telescope diameter and the baseline (Mariotti 1993; Conan et al. 2000; Ziad et al. 2004; Maire et al. 2006). Indeed, the optical path difference between the arms of an interferometer is more sensitive to the seeing for baselines shorter than the outer scale but for longer baselines, the outer scale dominates.

On the other hand, to reach a suitable limiting magnitude with a multi-aperture interferometer, we need to cophase the different telescopes using a reference source. This source should be located in the same isopistonic domain as the science source, which means that the differential atmospheric piston, within certain specifications, is the same in the direction of the two objects. The anisopistonic domain is directly related to the seeing conditions and an analytical expression is now available leading to the isopistonic angle from the Fried parameter, the isoplanatic angle and the outer scale (Elhalkouj et al. 2008).

In this paper, we provide the first statistics of the isopistonic angle at the major sites over the world (Section 3). These statistics are provided from the Generalized Seeing Monitor (GSM) data base (Ziad et al. 2000). The theoretical background on the isopistonic angle and particularly the relation to the other atmospheric turbulence parameters is given in Section 2. Implications on interferometry in terms of sky coverage and limiting magnitude of LBI cophasing are discussed in Section 5.

2 THEORETICAL BACKGROUND

To cophase different telescopes of an interferometer using a reference source (Mariotti 1993) requires that the latter should be located in the isopistonic domain around the science object. This means that differential atmospheric piston, within certain criteria, is the same in the direction of both objects. The isopistonic angle θ_p is defined as the angular radius of a circular region where the anisopistonic error reduces the visibility in the image plane to no more than 80 per cent of the unperturbed value (Esposito, Riccardi & Femenía 2000); this corresponds to a residual piston error σ_p about $\lambda/10$, where λ is the wavelength.

The definition for the isopistonic angle θ_p adopted here corresponds to the angular value $\theta = \theta_p$ which is reached when the residual piston error is equal to the desired accuracy $\sigma_p(\theta_p) = \lambda/n$, where n is an integer.

In the case of long baseline interferometers [KECK, VLTI, Large Binocular Telescope (LBT) . . .], we demonstrated in a recent study

⋆ E-mail: Aziz.ZIAD@unice.fr (AZ); t.elhalkouj@uca.ma (TE); romain.petrov@unice.fr (RGP)

(Elhalkouj et al. 2008) using some approximations that the squared residual piston error, could be simply written. Among these approximations, we consider high-altitude layers dominating on isoplanatic (Roddier 1981) and isopistonic angles and due to sky coverage and limiting magnitude, the angular position θ of reference star was assumed large. Thus, in the case of long baseline interferometers (even if the LBT is considered which has the smallest baseline 14.4 m) the distance $h\theta$ is in general much smaller than the baseline (Elhalkouj et al. 2008). Then, using these assumptions we can simplify the squared residual piston error as

$$\sigma_{\rm p}^2(\theta) = 3\pi^{2/3} D^{5/3} \int_0^\infty \int_0^\infty {\rm d}x{\rm d}h \frac{J_1^2(x) C_N^2(h)}{x \left[x^2 + \left(\pi \frac{D}{\mathcal{L}_0}\right)^2\right]^{\frac{11}{6}}} \times \left[1 - J_0\left(2x\frac{h\theta}{D}\right)\right], \quad (1)$$

where $\mathcal{L}_0$ indicates the wavefront spatial coherence outer scale, C_N^2 is the refractive index structure constant, D is the telescope diameter, h is the altitude and J_n is the Bessel function of order n. One can remark as demonstrated in the first paper (Elhalkouj et al. 2008), this variance expression is not function of the baseline B of the interferometer. This is due that in the case of large interferometers considered here, the spatial correlation is governed by the outer scale which is smaller than the baseline B.

This approximative expression has been validated numerically in different conditions particularly for unfavourable case with short baseline as LBT interferometer (Elhalkouj et al. 2008).

The integral in equation (1) can be expressed simply with convergent series using Mellin transform (Sasiela 1994). Two simple analytical expressions are now available for the isopistonic variance for small and large apertures (Elhalkouj et al. 2008):

(i) For $D \leq 1.3\frac{\mathcal{L}_0}{\pi}$ and $D \geq 3\,h_{\rm max}\,\theta_0$:

$$\sigma_{\rm p}^2(\theta) = 8.8\,10^{-2}\,\pi^{2/3}\lambda^2 \left(\frac{D}{r_0}\right)^{-\frac{1}{3}} \times \left(\frac{\theta}{\theta_0}\right)^2 \left[0.216 - 0.225\left(\frac{\pi D}{\mathcal{L}_0}\right)^{1/3} + 0.122\left(\frac{\pi D}{\mathcal{L}_0}\right)^2 - 0.096\left(\frac{\pi D}{\mathcal{L}_0}\right)^{7/3} + 0.02\left(\frac{\pi D}{\mathcal{L}_0}\right)^4 - 0.014\left(\frac{\pi D}{\mathcal{L}_0}\right)^{13/3}\right] \quad (2)$$

(ii) For $D > 1.3\frac{\mathcal{L}_0}{\pi}$ and $D \geq 6\,h_{\rm max}\,\theta_0$:

$$\sigma_{\rm p}^2(\theta) = 5.9\,10^{-3}\,\pi^{2/3}\lambda^2 \left(\frac{D}{r_0}\right)^{-\frac{1}{3}} \left(\frac{\theta}{\theta_0}\right)^2 \times \left[\left(\frac{\pi D}{\mathcal{L}_0}\right)^{-8/3} - \left(\frac{\pi D}{\mathcal{L}_0}\right)^{-14/3}\right], \quad (3)$$

where $h_{\rm max}$ is the highest altitude of C_N^2 profile [$h_{\rm max}$ depends on the turbulence conditions and it is lower than 30 km for radio-sounding balloons (Abahamid et al. 2004)]. In the rest of this paper, $h_{\rm max}$ is fixed to 20 km in coherence with Elhalkouj et al. (2008) and considering that turbulence beyond this altitude is negligible. The Fried parameter is indicated by r_0 and θ_0 corresponds to the isoplanatic angle. One can see that in both cases the expression of $\sigma_{\rm p}^2(\theta)$ does not require C_N^2 profiles but it is directly related to the total turbulence energy characterized by the Fried parameter r_0.

Using the criterion of the isopistonic angle definition $\sigma_{\rm p}(\theta_{\rm p}) = \frac{\lambda}{n}$ and $\sigma_{\rm p}^2(\theta)$ expression given by equation (2) or (3), the general expression of isopistonic angle is given by Elhalkouj et al. (2008):

(i) Small-aperture case : $D \leq 1.3\,\mathcal{L}_0/\pi$ and $D \geq 3\,h_{\rm max}\theta_0$

$$\theta_{\rm p} = \frac{2.3}{n}\theta_0 \left(\frac{D}{r_0}\right)^{1/6} \left[0.216 - 0.225\left(\frac{\pi D}{\mathcal{L}_0}\right)^{1/3} + 0.122\left(\frac{\pi D}{\mathcal{L}_0}\right)^2 - 0.096\left(\frac{\pi D}{\mathcal{L}_0}\right)^{7/3} + 0.02\left(\frac{\pi D}{\mathcal{L}_0}\right)^4 - 0.014\left(\frac{\pi D}{\mathcal{L}_0}\right)^{13/3}\right]^{-1/2} \quad (4)$$

(ii) Large-aperture case: $D > 1.3\,\mathcal{L}_0/\pi$ and $D \geq 6\,h_{\rm max}\theta_0$

$$\theta_p = \frac{8.9}{n}\theta_0 \left(\frac{D}{r_0}\right)^{1/6} \left[\left(\frac{\pi D}{\mathcal{L}_0}\right)^{-8/3} - \left(\frac{\pi D}{\mathcal{L}_0}\right)^{-14/3}\right]^{-1/2}. \quad (5)$$

Here, the atmospheric turbulence parameters r_0 and θ_0 are considered in their standard definitions where the effect of the outer scale is not taken into account (Roddier 1981).

3 STATISTICS OF ISOPISTONIC ANGLE

3.1 GSM instrument

The GSM instrument (Fig. 1) consists of evaluating the atmospheric optical parameters (AOP) of the perturbed wavefront by measuring angle of arrival (AA) fluctuations. Indeed, the GSM uses the same principle than a Shack–Hartmann, i.e. measuring AA at different points of the wavefront and computing AA spatio-temporal correlations leads to estimates of the seeing ϵ_0, outer scale $\mathcal{L}_0$, isoplanatic angle θ_0 and coherence time τ_0.

The standard version of the GSM instrument consists of four 10 cm telescopes on equatorial mounts equipped with detection modules measuring the AA fluctuations and interfaced to a computer PC managing simultaneously the four modules (Fig. 1). Each telescope, pointing at the same star, measures the AA fluctuations by means of flux modulation which is produced by the displacement of the star image over a Ronchi grating. Two telescopes are installed on a common mount on a central pier working as a differential image motion monitor (DIMM) with a 25 cm baseline. Two other telescopes have different mounts on separate piers, located 0.8 m to the south and 1 m to the east from the central pier, thus forming an L-shaped configuration. This configuration has been chosen for more sensitivity to the outer scale. The telescopes were situated 1.7 m above the ground.

The GSM version installed at Dome C is based on two identical DIMMs simultaneously observing the same star (Ziad et al. 2008). Each DIMM is a telescope equipped with a mask having sub-apertures of 6 cm diameter separated by 20 cm. In the configuration of the GSM at Dome C, the distance between the telescopes is 1 m in the north–south direction when the observed star transits at the meridian. Before and after the star transit, the sub-apertures of the two telescopes are not aligned and the baselines depend on the star position. A projection of these ground baselines on the wavefront plane is performed as described by Avila et al. (1997). The AA measurement in the X-direction is aligned with the declination δ and with right ascension α in the Y-direction. As the star diurnal movement compensation by the mounts is in α, we decided to avoid the Y-direction AA measurement which is contaminated by the vibrations due to the mount driving.

Figure 1. Standard GSM working layout at La Silla (Chile) 1997 September.

The AA fluctuations are measured with 5 ms resolution time during 2 min acquisition time. For the Dome C version, the exposure time was lower than 5 ms (Ziad et al. 2008). Data are processed immediately after each acquisition, allowing a quasi-real-time monitoring of the AOP. The data acquisition is repeated typically every 4 min.

The AA covariances are computed for each baseline and normalized by the differential variance of AA on the 20 or 25 cm baseline (respectively, for Dome C and standard GSM). They are compared to von Kàrmàn theoretical normalized covariances (Avila et al. 1997) and the appropriate $\mathcal{L}_0$ is found for each baseline. The final value of $\mathcal{L}_0$ is taken as the median of the individual $\mathcal{L}_0$ values and its error is estimated. The seeing ϵ_0 is calculated from the differential variance given by the DIMM method (Sarazin & Roddier, 1990). The scintillation index σ_I^2 is computed during data reduction and an estimate of the isoplanatic angle is deduced (Ziad et al. 2000).

A quantification of the different GSM noises has been performed and hence corrections of photon and scintillation noises are done before data processing. Another correction for finite exposure time is also performed for the GSM standard version; it consists in computing AA variance (or covariance) for 5 and 10 ms and in extrapolating linearly to the 0 ms exposure time. For the Dome C, thanks to the low wind speed, the coherence time is particularly large as compared with other observatories (Trinquet et al. 2008). And as the exposure time for the GSM at Dome C was smaller than 5 ms, its effect was negligible. Finally, the statistical errors of the computed variances and covariances are estimated and consequently the errors of the AOP measured with GSM are provided.

In order to check the wind shake effect, r_0 is computed from absolute image motion in each telescope (variance of AA fluctuations), corrected for finite $\mathcal{L}_0$ (Ziad et al. 1994) and compared to r_0 provided by the differential technique. A good agreement is found for ground wind speed less than 10 m s^{-1} (3–4 m s^{-1} for Dome C), showing that telescope vibrations were not significant.

3.2 Isopistonic data

Using the Mellin transform, an analytical expression has been developed by Elhalkouj et al. (2008) for the differential piston variance depending on the accessed Fried parameter r_0 instead of C_N^2 profiles. This expression enables us to establish a new direct formula for the isopistonic angle θ_p as an analytical function of the isoplanatic angle θ_0, the Fried parameter r_0, the atmospheric outer scale $\mathcal{L}_0$, and the aperture diameter D (Section 2). This formula is then used to fill the gap in isopistonic angle measurements. We have two analytical expressions (equations 4 and 5) corresponding to small and large aperture cases. Then, using the data base of the site-testing parameters with the GSM instrument from 1997 to 2006, first statistics of θ_p were deduced and presented in Figs 2 and 3 for 8 m telescope at 0.5 μm. The atmospheric turbulence parameters provided by the GSM instrument are obtained for an integration time of 2 min and are corrected from exposure time (Section 3.1).

Fig. 2 shows the night-by-night θ_p statistics at $\lambda/10$ accuracy of the Paranal campaign in 1998 November/December. Each night is represented by its cumulative distribution where one can read easily the median value corresponding to the 50 per cent cut. The number of data points is also indicated. The interest of this campaign is that all the situations are present. Indeed, some nights are very homogeneous presenting a weak data dispersion. For example, the nights of December 14 and 20 where 100 per cent of the values are included respectively in the intervals 1.93–10.53 arcsec and 2.32–10.6 arcsec. During these nights, the isopistonic domain was relatively tight. Contrary, the night of November 28 presents a large dispersion with a median value of ∼13.5 arcsec corresponding to a large isopistonic domain.

Fig. 3 shows the whole campaign histograms of θ_p at $\lambda/10$ accuracy obtained at the different sites for 8 m telescope at $\lambda = 0.5$ μm. Statistics on the seeing conditions obtained by GSM during these campaigns are given by Ziad et al. (2000, 2008). All these histograms are well fitted with lognormal distributions. One can remark that all these sites have tight isopistonic domains relatively to the Dome C in Antarctica. Beside this conclusion, direct comparisons between other sites is not representative of the whole behaviour of these sites because of the difference in the observation conditions (campaign period and duration). From the GSM data, the Dome C site presents the best conditions of isopistonic domain and obviously of other seeing parameters (Aristidi et al. 2009). In addition to the good seeing, the outer scale is at least 2 times lower than other sites (Ziad et al. 2008) and the isoplanatism range is large. The isopistonic angle at Dome C is more than 5 times larger than at Paranal, which relaxes the interferometer cophasing in terms of sky coverage. However, we have to put these conclusions in perspective due to the presence of a dominant surface layer leading to a small outer scale and also for the very difficult access to this site.

Fig. 4 shows the logarithmic median values of the isopistonic angle for telescopes of $D = 2$ m (red line) and $D = 10$ (blue line) at $\lambda = 2.2$ μm. Each site is represented by the θ_p median value

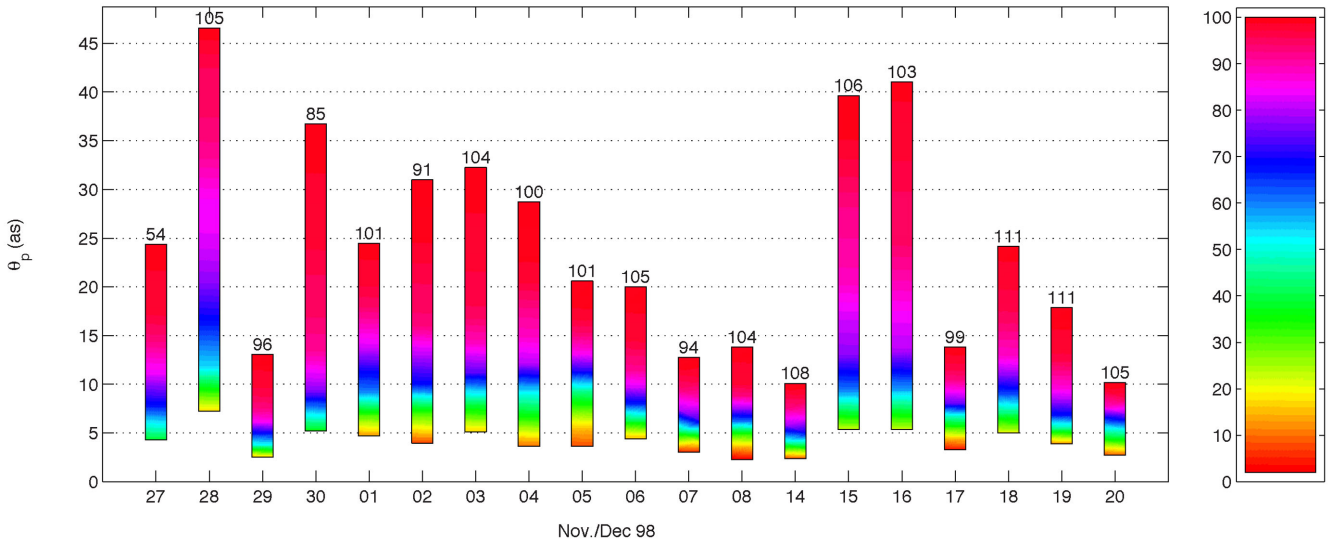

Figure 2. Summary of the isopistonic angle θ_p statistics at $\lambda/10$ accuracy for the Paranal campaign (1998 November/December) and 8 m telescope at $\lambda = 0.5$ µm. For each night, the cumulative distribution of θ_p is shown and the corresponding data number is indicated. Each data correspond to 2 min acquisition time.

and the error bars correspond to the standard deviation of $log(\theta_p)$ data. Once again, one can remark that the Dome C presents a large isopistonic domain. One has to recall that θ_p is proportional to the wavelength λ. Then, it is easy to deduce θ_p at all wavelengths from seeing conditions measured at $\lambda = 0.5$ µm.

4 TEMPORAL STABILITY OF THE ISOPISTONIC ANGLE

It is important for long baseline interferometry to characterize the temporal evolution of the well-known turbulence optical parameters. This temporal stability is particularly fundamental to know how long the isopistonic angle remains constant. This issue has been analysed by Racine (1996) concerning the seeing prediction and for scheduling astronomical programmes. To analyse this temporal variability, it was suggested to use the normalized difference (ND) of two seeing measurements separated with a time delay Δt (Racine 1996). This ND applied to the isopistonic measurements leads to

$$ND(\Delta t) = \left\langle \frac{|\theta_p(t+\Delta t) - \theta_p(t)|}{[\theta_p(t+\Delta t) + \theta_p(t)]} \right\rangle . \quad (6)$$

Fig. 5 shows this *ND* evolution in the case of isopistonic measured at La Silla Observatory in 1997 August/September. The choice of La Silla data is justified by the fact that the temporal stability of outer scale, seeing and isoplanatic angle published by Ziad et al. (2012) have been analysed with the same data which allows direct comparisons. The GSM data at La Silla have been obtained over 16 nights (1418 data) with a high data density for each night. Indeed, for this first GSM campaign, we obtained during the observations a reduced lost time (star change, clouds, mechanical problems on mounts...). We first calculated the ND function in equation (6) for each night and then an average over the 16 nights lead to the result presented in Fig. 5. The first remark is that the amplitude of this relative difference in the case of the isopistonic angle is comparable to the outer scale $\mathcal{L}_0$ and more important comparatively to the seeing ϵ_0 and to the isoplanatic angle θ_0 (Ziad et al. 2012). This saturated ND-curve in Fig. 5 could be fitted by an appropriate function defined by Racine (1996) as $ND(\Delta t) = ND_s\,(1 - exp(-\Delta t/\tau))$; where ND_s is the saturation value of *ND* and τ is the e-folding time. This function was used to fit the data by least squares minimization as is shown in dark dashed line in Fig. 5. Then, it was found for the θ_p an e-folding time of $\tau_p = 8.8$ min which is comparable to the outer scale one but smaller than the seeing one (Ziad et al. 2012).

5 IMPLICATIONS ON INTERFEROMETRY

In long baseline interferometry, the cophasing on an off-axis source is crucial, especially for the detection and study of fainter objects (targets of GRAVITY at VLTI for example). Indeed, for this kind of observations, the flux is so weak that it is impossible to split it for cophasing. Then, cophasing on a reference source other than scientific object is required. This leads to two major constraints related to the sky coverage issue; first, we have to find a reference source bright enough for cophasing. The second constraint is related to the isopistonic domain. Indeed, the anisopistonic error, i.e. the difference between the pistons on the off-axis reference and the science source, increases with their separation distance. This error of the differential piston is giving by its variance in equations (2) and (3) which leads to an anisopistonic domain characterized by the isopistonic angle θ_p defined by equations (4) and (5).

The total error which intervenes when cophasing an interferometer is given by

$$\sigma^2_{\rm total} = \sigma^2_p + \sigma^2_\varphi, \quad (7)$$

where σ^2_p is the anisopistonic error and σ^2_φ is the error on the phase of the Fourier transform of the interferogram. For simplicity, we did not consider here the fringe tracking loop error.

In the pairwise approach, the error on the phase for an unresolved star and in the case of weak flux ($\Gamma << \Lambda + N^2_{p0}\,\sigma^2_R$), is given by Elhalkouj (2008), Petrov, Roddier & Aime (1986) and Vannier et al. (2006):

$$\sigma^2_\varphi = \frac{\lambda^2}{2\pi^2}\left[\frac{\Lambda}{\Gamma^2} + \frac{N^2_{p0}\,\sigma^2_R}{\Gamma^2}\right], \quad (8)$$

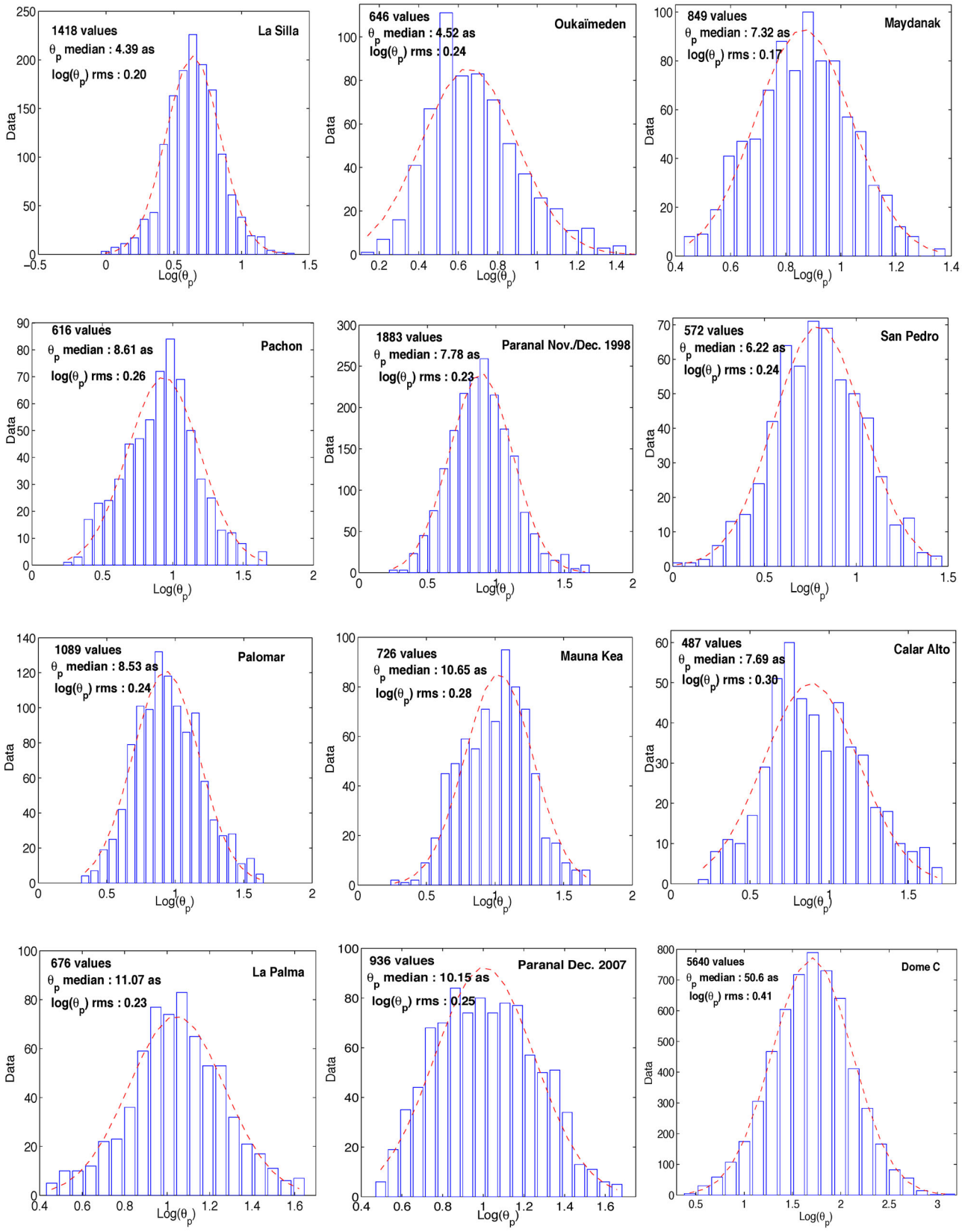

Figure 3. Isopistonic angle histograms at $\lambda/10$ accuracy for 8 m telescope and $\lambda = 0.5$ μm obtained during the different campaigns performed with the GSM instrument. The median θ_p is deduced from the best fit with a log-normal distribution. Each data correspond to 2 min acquisition. From left to right and top to bottom: La Silla, Oukaïmeden, Maydanak, Cerro Pachon, Paranal (1998 November/December), San Pedro Mártir, Palomar, Mauna Kea, Calar Alto, La Palma, Parental (2007 December) and Dome C.

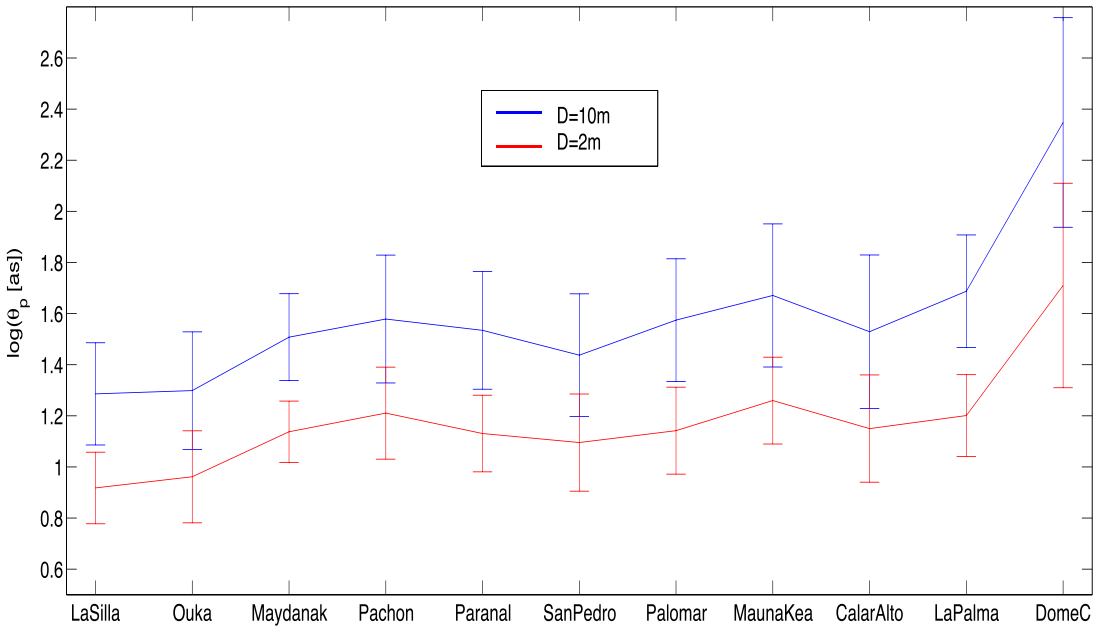

Figure 4. Isopistonic angle $\theta_{\rm p}$ statistics at $\lambda/10$ accuracy for different telescope diameters $D = 2$ and 10 m in the K band at $\lambda = 2.2$ μm. Each site, is represented by its logarithmic median value $log(\theta_{\rm p})$ and error bars correspond to the standard deviation of data.

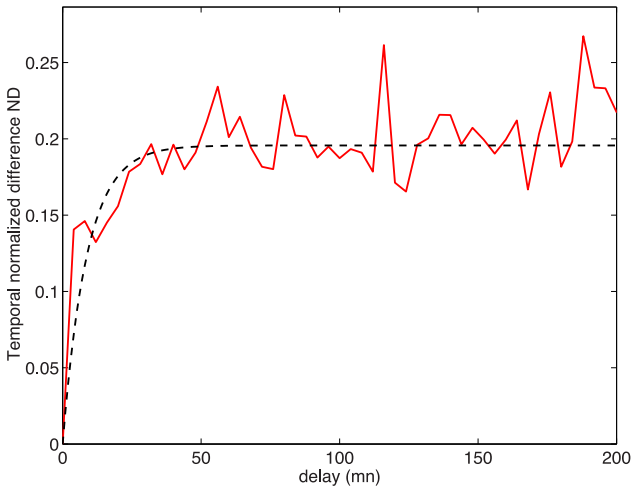

Figure 5. The temporal normalized difference *ND* of the estimated isopistonic angle θ_p obtained with GSM data at La Silla Observatory in August/September 1997.

where $N_{\rm p0}$ is the number of pixels necessary to sample the interferogram and $\sigma_{\rm R}^2$ is the variance of the detector read out noise. Γ and Λ are the total source and thermal background fluxes contributing to an interferogram.

On the other hand, the magnitude m_K in the K band is obtained from the following relation (Léna, Lebrun & Mignard 1995)

$$\Gamma = 4\ T_r S_R \delta\lambda \tau\, D^2 10^{5-0.4\, m_K}\,, \ \delta\lambda \text{ is in Å unit,} \tag{9}$$

where $S_{\rm R}$ is the Strehl ratio, T_r the atmospheric and instrumental transmission, $\delta\lambda$ is the spectral bandwidth and τ the exposure time.

Thus, equation (8) can be written in term of the magnitude m_K as:

$$\sigma_\varphi^2 = \lambda^2\ F\ \times 10^{\frac{4}{5}\, m_K}, \tag{10}$$

where,

$$F = \frac{\Lambda + N_{\rm p0}^2\ \sigma_{\rm R}^2}{32\ 10^{10}\pi^2\ S_r^2\ T_r^2\ \delta\lambda^2 \tau^2 D^4}. \tag{11}$$

It should be noted that the maximum exposure time τ is limited by the temporal decorrelation of the atmosphere reducing the fringe contrast of each exposure.

The mean density of stars (number of stars per rad^2) in K band around the Galactic pole is given by Elhalkouj (2008):

$$\alpha(m_K) = 290 \times 10^{\frac{m_K}{4}}. \tag{12}$$

Then, combining equations (7), (10) and (12), leads to:

$$\alpha(m_K) = 290 \times \left[\frac{1}{\lambda^2 F}(\sigma_{\rm total}^2 - \sigma_{\rm p}^2)\right]^{5/16}. \tag{13}$$

In the literature, the sky coverage is only related to the star density in the sky. However, it is clear that the ability to detect a reference star depends also on the instrument, the atmospheric conditions and on the isopistonic domain. In this context, we can deduce the sky coverage Ω using the expression of the above magnitude.

$$\Omega = \int_0^{\theta_{\rm p}} {\rm d}\theta\ 2\pi\ \theta\ \alpha(m_K)\ . \tag{14}$$

After integration and for a total error of $\sigma_{\rm total} = \lambda/n$ as in the case of isopistonic domain, this expression leads to

$$\Omega = \frac{221}{n^{5/8}} \frac{\pi}{F^{5/16}}\ \theta_{\rm p}^2. \tag{15}$$

Fig. 6 shows the role played by the isopistonic domain in the sky coverage in the case of Paranal site in K band. We considered, the median and standard deviation values of $\theta_{\rm p}$ corresponding to December 2007 campaign (Fig. 3). The instrumental parameters correspond to the VLTI/AMBER with $S_r = 50$ per cent, $T_r = 1$ per cent, $\delta\lambda = 4000$ Å and $\Lambda = 0$. We consider pixel number limited to $N_{\rm p0} = 5$ (Petrov et al. 2014).

Current fringe trackers on Paranal with the VLTI-UTs and on Mauna Kea with the KECK Interferometer have achieved fringe

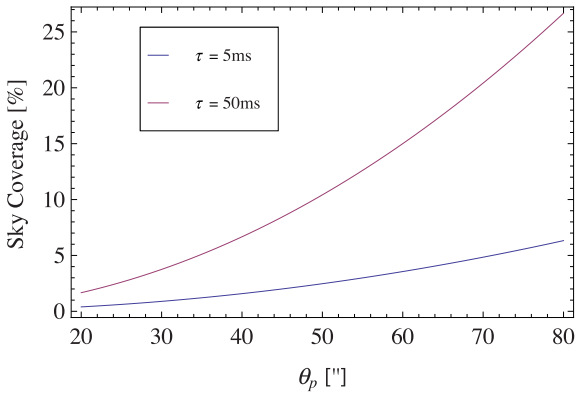

Figure 6. Sky Coverage (at galactic pole) versus isopistonic angle in *K* band and Paranal conditions for exposure times $\tau = 5$ and 50 ms, respectively, in blue and red.

Table 1. Sky coverage Ω at galactic pole for different limiting magnitude m_K and visibilities in Paranal conditions at $\lambda = 2.2$ μm.

Visibility	$0.57(n = 6)$	$0.95(n = 20)$
Ω at $m_K = 10$	1.8 per cent	0.16 per cent
Ω at $m_K = 13$	10.0 per cent	0.90 per cent

tracking magnitude of $m_K \sim 10$ in good seeing conditions. The best expectation with current technologies for fringe tracker of the VLTI second-generation instruments (GRAVITY), we should achieve $m_K = 10.5$ in median Paranal conditions using a SELEX detector (Choquet et al. 2012). New fringe tracker concepts, optimized for large spectral bands and using a smaller number of pixels, such as the NOVA fringe tracker (Meisner, Walter & Le Poole 2012) or the hierarchical fringe tracker (Elhalkouj et al. 2006; Petrov et al. 2014), could reach $m_K > 13$ for the VLTI. A full discussion on fringe trackers performance is beyond the scope of this paper, and here we discuss the sky coverage with these two m_K fringe tracking limiting magnitudes. Indeed, for the two values of limiting magnitude above, one can estimate the sky coverage that we should expect at Paranal. For this, we consider two cases with good contrast which corresponds to 95 per cent of visibility ($\lambda/20$ accuracy)[1] and medium contrast corresponding to 57 per cent of visibility ($\lambda/6$ accuracy). Then, under hypothesis that the instrumental and anisopistonic errors have an equivalent contribution in the total error $\sigma^2_{\rm total}$, one has $\sigma^2_\phi = \sigma^2_{\rm p} = \frac{\lambda^2}{2\,n^2}$. Thus, the instrumental error leads to the exposure time to reach the limiting magnitude of m_K while the anisopistonic error leads to $\theta_{\rm p}$. The sky coverage Ω at galactic pole is shown in Table 1 in the conditions of Paranal site (Fig. 3) at $\lambda = 2.2$ μm.

In young stars region, at 20° of galactic declination, the star density is about 10 times greater than that at the galactic pole (Elhalkouj 2008). Therefore the sky coverage becomes greater as shown in Table 2. One can see that a cophasing magnitude $m_K \sim 13$ is sufficient to have a full sky coverage in the two nearest young star groups (Orion or Tauri constellation), which has a decisive impact on the young star and young planetary disc programmes with the VLTI second-generation instruments GRAVITY and Multi AperTure mid-Infrared SpectroScopic Experiment (MATISSE).

[1] The limiting magnitude $m_K \sim 10$ for GRAVITY corresponds to an SNR = 1 (i.e. phase error of ∼1 rad and piston error of $\sim\lambda/6$) per frame, spectral channel and polarization. This is also the condition to add coherently the information from all channels. As we have five spectral channels, two polarizations and six baselines to measure three pistons, the overall piston error will be divided by $\sqrt{5 * 2 * (6/3)}$ that yields to $\lambda/27$. For the hierarchical fringe tracker, the extrapolation based on the number of used pixels, channels and bandwidth yields to $\lambda/6$ for about m_K 14.5, i.e. $\lambda/30$ for m_K 13, if the fringe tracking accuracy is limited only by the atmospheric piston and the photon, background and detector noises.

Table 2. Sky coverage Ω at 20° of galactic declination (Orion or Tauri constellation) for different limiting magnitude m_K and visibilities in Paranal conditions at $\lambda = 2.2$ μm.

Visibility	$0.57(n = 6)$	$0.95(n = 20)$
Ω at $m_K = 10$	18 per cent	1.6 per cent
Ω at $m_K = 13$	100 per cent	9 per cent

6 CONCLUSIONS

For the first time, statistics of the isopistonic angle are now available for the major observatories around the world, thanks to the GSM data base of atmospheric turbulence parameters as seeing, isoplanatic angle and outer scale. Indeed, a direct analytical expression is now available deducing the isopistonic angle from the atmospheric turbulence parameters. Due to a prevailing surface layer and a large isoplanatic angle, Dome C in Antarctica seems to be more favourable for isopistonic domain. But we have to put this conclusion in perspective due to Dome C dominant surface layer leading to small outer scale and also for the extreme conditions of this site. The isopistonic angle is proportional to the wavelength leading to a generalized statistics for each λ. Stability time of the isopistonic angle is comparable to the outer scale and isoplanatic ones. Implications of the isopistonic angle statistics on multi-aperture interferometer cophasing in terms of sky coverage and limiting magnitude in different instrumental conditions of the VLTI, are shown leading to the importance of the anisopistonic error when cophasing on off-axis reference star.

REFERENCES

Abahamid A., Jabiri A., Vernin J., Benkhaldoun Z., Azouit M., Agabi A., 2004, A&A, 416, 1193
Aristidi E. et al., 2009, A&A, 499, 955
Avila R., Ziad A., Borgnino J., Martin F., Agabi A., Tokovinin A., 1997, J. Opt. Soc. Am., 14, 3070
Choquet E., Abuter R., Menu J., Perrin G., Fédou P., 2012, in Delplancke F., Rajagopal J. K., Malbet F., eds, Proc. SPIE Conf. Ser. Vol. 8445, Optical and Infrared Interferometry III. SPIE, Bellingham, p. 8
Conan R., Ziad A., Borgnino J., Martin F., Tokovinin A., 2000, in Lena P. J., Quirrenbach A., eds, Proc. SPIE Conf. Ser. Vol. 4006, Interferometry in Optical Astronomy. SPIE, Bellingham, p. 963
Elhalkouj T., 2008, PhD thesis, Univ. Cadi Ayyad, Marrakesh
Elhalkouj T., Petrov R. G., Lazrek M., Ziad A., Benkhaldoun Z., 2006, in Monnier J. D., Schöller M., Danchi W. C., eds, Proc. SPIE Conf. Ser. Vol. 6268, Advances in Stellar Interferometry, SPIE, Bellingham, p. 626812
Elhalkouj T., Ziad A., Petrov R. G., Lazrek M., Elazhari Y., Benkhaldoun Z., 2008, A&A, 477, 337
Esposito S., Riccardi A., Femenía B., 2000, A&A, 353, L29
Léna P., Lebrun F., Mignard F., 1995, Méthodes Physiques de l'Observation. CNRS Editions, Paris
Maire J., Ziad A., Borgnino J., Mourard D., Martin F., Jankov S., Bonneau D., Patru F., 2006, A&A, 448, 1225
Mariotti J., 1993, in Alloin D., Mariotti J. M., eds, Adaptive Optics for Astronomy. Kluwer, Dordrecht, p. 309

Meisner J. A., Walter J., Le Poole R. S., 2012, in Delplancke F., Rajagopal J. K., Malbet F., eds, Proc. SPIE Conf. Ser. Vol. 8445, Optical and Infrared Interferometry III. SPIE, Bellingham, p. 22
Petrov R. G., Roddier F., Aime C., 1986, J. Opt. Soc. Am., 3, 634
Petrov R. G., Elhalkouj T., Boskri A., Folcher J. P., Lagarde S., Bresson Y., Benkhaldoun Z., Lazrek M., 2014, in Rajagopal J. K., Creech-Eakman M. J., Malbet F., Proc. SPIE Conf. Ser. Vol. 9146, Optical and Infrared Interferometry IV. SPIE, Bellingham, p. 101
Racine R., 1996, PASP, 108, 372
Roddier F., 1981, in Wolf E., ed., Progress in Optics, Vol. XIX, The effect of atmospheric turbulence in optical astronomy. North-Holland Publishing Co., Amsterdam, p. 337
Sarazin M., Roddier F., 1990, A&A, 227, 294
Sasiela R. J., 1994, in Brekhovskikh L. M., Felsen L. B., Haus H. A., eds, Electromagnetic Wave Propagation in Turbulence, Evaluation and Application of Mellin Transforms. Springer-Verlag, Berlin
Trinquet H., Agabi A., Vernin J., Azouit M., Aristidi E., Fossat E., 2008, PASP, 120, 203
Vannier M., Petrov R. G., Lopez B., Millour F., 2006, MNRAS, 367, 825
Winker D., 1991, J. Opt. Soc. Am. A, 8, 1568
Ziad A., Borgnino J., Martin F., Agabi A., 1994, A&A, 282, 1021
Ziad A., Conan R., Tokovinin A., Martin F., Borgnino J., 2000, Appl. Opt., 39, 5415
Ziad A., Schöck M., Chanan G. A., Troy M., Dekany R., Lane B. F., Borgnino J., Martin F., 2004, Appl. Opt., 43, 2316
Ziad A., Aristidi E., Agabi A., Borgnino J., Martin F., Fossat E., 2008, A&A, 491, 917
Ziad A., Borgnino J., Dali Ali W., Berdja A., Maire J., Martin F., 2012, J. Opt., 14, 045705

This paper has been typeset from a TEX/LATEX file prepared by the author.